Optics Letters

Magneto-optical effects in hyperbolic metamaterials

I. A. Kolmychek,[1,*] A. R. Pomozov,[1] A. P. Leontiev,[2] K. S. Napolskii,[2,3] and T. V. Murzina[1]

[1]Department of Physics, M. V. Lomonosov Moscow State University, Leninskie Gory, Moscow 119991, Russia
[2]Department of Materials Science, M. V. Lomonosov Moscow State University, Leninskie Gory, Moscow 119991, Russia
[3]Department of Chemistry, M. V. Lomonosov Moscow State University, Leninskie Gory, Moscow 119991, Russia
*Corresponding author: irisha@shg.ru

Received 9 May 2018; revised 10 July 2018; accepted 11 July 2018; posted 19 July 2018 (Doc. ID 331275); published 8 August 2018

Highly anisotropic metal-dielectric structures reveal unique dispersion properties providing new optical effects. Here we study experimentally linear optical and magneto-optical response of arrays of plasmonic gold nanorods and similar structures complemented by a thin nickel film. We show that both types of structures reveal distinct optical features expected for hyperbolic media and associated with the epsilon-near-zero (ENZ) and epsilon-near-pole (ENP) points. In the case of Ni-containing nanocomposites, we observe linear magneto-optical effects in transmission through the structure, increasing in the vicinity of these points. This observation reveals an important role of the local field enhancement in a hyperbolic medium associated with ENZ and ENP dispersion points in the appearance of magneto-optical activity of magnetic hyperbolic metamaterials.

OCIS codes: (160.3820) Magneto-optical materials; (160.3918) Metamaterials; (240.6680) Surface plasmons.

https://doi.org/10.1364/OL.43.003917

Hyperbolic metamaterials (MMs) attract great attention because of their unique dispersion governed by a strong anisotropy of the metal-dielectric architecture [1–4]. Two types of critical dispersion points that correspond to zero and infinite values of the dielectric permittivity, respectively, provide resonant optical behavior of a MM that can be tuned by a proper choice of the constituting materials, spacing between the nanoelements, their relative composition, etc. Up to now, many works have been devoted to studies of the optical response of hyperbolic MMs consisting of an ordered array of metal nanorods with a high aspect ratio disposed in a dielectric host material [5]. In this case, the effective dielectric constant can be described by two components that correspond to the directions parallel ($\varepsilon_{\|}$) and perpendicular ($\varepsilon_{\perp}$) to the long axis of nanorods, respectively, so that the isofrequency surface for the TM mode is given by the hyperbolic function

$$\frac{k_x^2 + k_y^2}{\varepsilon_{\|}} + \frac{k_z^2}{\varepsilon_{\perp}} = \left(\frac{\omega}{c}\right)^2. \quad (1)$$

Here ω is the frequency of the electromagnetic wave, $k_{x,y,z}$ are the related components of the wave vector that are introduced in a coordinate system associated with the MM, c is the speed of light. In the case of a metal-dielectric nanocomposite consisting of nanorods with the z-direction parallel to the rod's axis, the related component of the effective dielectric permittivity $\varepsilon_{\|} = \varepsilon_{zz}$ is described by the resonant function [1,2]

$$\varepsilon_{\|} = 1 - \frac{\Omega_p^2}{\omega^2 - \delta^2 - c^2 k_z^2}, \quad (2)$$

where Ω_p is the plasma frequency, and δ is a constant determined by parameters of the constituting materials, aspect ratio, and geometry of nanorods. It stems from Eq. (2) that for definite k_z value, $\varepsilon_{\|}$ can pass through zero and become negative, thus approaching the hyperbolic regime. This critical point is referred to as epsilon-near-zero (ENZ). Close to this point, one may expect a strong amplification of the electromagnetic field inside the MM and relevant enhancement of optical effects such as the Purcell effect [6], subwavelength focusing and imaging [7], and efficiency of the nonlinear optical processes [8,9]. A critical point of another type corresponds to a pronounced increase of the real part of the dielectric permittivity of a MM and, therefore, is recalled as epsilon-near-pole (ENP). It corresponds to the restricted motion of electrons in the direction perpendicular to the nanorods and can be referred to as localized plasmon excitation [5]. Its spectral position revealed by the absorption maximum is independent of the geometry of the light-matter interaction. A special interest is attracted to hyperbolic MMs containing magnetic specimens. Being combined with specific features noted above, these types of MMs are especially attractive [5,10].

Nearly the simplest way for the fabrication of the MM composed of an array of nanorods is the electrochemical deposition of metal (gold, silver, etc.) in a porous anodic alumina membrane composed by anodization [5]. As a ferromagnetic metal is deposited inside the pores, one gets a magnetic MM with a possibility for the magnetic field control over its optical properties. Here one may expect a pronounced amplification of the magneto-optical response, similar to that demonstrated recently for various resonant structures such as arrays of plasmonic nanoparticles in a magnetic dielectric [11,12],

magneto-plasmonic crystals with surface plasmon polariton resonances attained at the interface of a magnetic dielectric with a noble metal [13,14], and arrays of nickel nanorods [15] in the spectral vicinity of the localized surface plasmon resonance that is the ENP point. Similar effects should be even more pronounced in the case of nonlinear optics due to local field effects [16,17]. At the same time, spectroscopic studies of magneto-optical effects in composite hyperbolic materials formed by a combination of noble and ferromagnetic metals have not been performed up to now. Here we study the optical response of MMs consisting of arrays of Au nanorods supplemented by a nickel film, with the emphasis on the spectroscopy of the linear magneto-optical effects. Numerical modelling of the permittivity tensor components and the local field effects in such structures supports the experimental results.

Arrays of gold nanorods in anodic aluminum oxide (AAO) matrices were prepared by templated electrodeposition. The AAO templates were obtained by two-step anodizing of aluminum (99.99%) in 0.3 M oxalic acid at 20°C. The thickness of the AAO films was controlled coulometrically using the thickness-to-charge density ratio of 480 nm cm^2 C^{-1}. At the first step, Al was anodized at a constant voltage of 40 V until the charge density of 20.9 C cm^{-2} was spent. Then a sacrificial alumina layer was selectively dissolved. The second anodizing was carried out in several stages. First, a 20 μm thick AAO layer was made at 40 V. Then the anodizing voltage was gradually increased to 80 V with a constant rate of 0.5 V s^{-1} and kept steady until the 1 μm thick AAO layer is formed. When the anodizing voltage increased, the average interpore distance grew up, and a part of the pores stopped growing, forming the blocked channels [18]. At the third stage, the anodizing voltage was decreased slowly to 40 V with a rate of 0.25 V s^{-1} and then kept constant until the total thickness of AAO film reached 50 μm.

Aluminum remained after the anodization was selectively dissolved in a mixture of Br_2 and CH_3OH taken with a volume ratio of 1:10. Then a continuous oxide layer at the pore bases was etched away chemically in 3 M solution of H_3PO_4 with electrochemical detection of a pore opening moment [19]. Finally, a 200 nm thick Cu layer serving as a current collector was deposited onto the top side of the templates using magnetron sputtering.

Electrodeposition of gold was carried out using commercial electrolyte 04-ZG (Ecomet, Russia) containing buffered $[Au(CN)_2]^-$ (pH = 6) as described elsewhere [20,21]. Au nanorods were formed at a constant potential of −1 V versus saturated Ag/AgCl reference electrode. The diameter of Au nanorods and the distance between the centers of neighbor nanorods coincide with the pore diameter (40 ± 4 nm) and interpore distance (101 ± 8 nm) of AAO, respectively. The length of the nanorods depends on the charge spent during electrodeposition and, in our case, was equal to 580 ± 40 nm. Before optical measurements, the Cu layer was etched away in a dilute nitric acid for 1 min. According to the scanning electron microscopy (SEM) studies, the volume fraction of metal in the Au/AAO nanocomposite is about 8% which is 2.4 times lower than the porosity of the AAO template. To the best of our knowledge, the approach of controlled blocking of the pores which provides the decrease of the template filling factor by metal and, thus, tunes the ENZ spectral position of the nanocomposite is applied here for the first time.

To obtain hyperbolic MM sensitive to the magnetic field, a continuous ferromagnetic 15 ± 3 nm thick Ni layer was deposited on the top side of the AAO template by magnetron sputtering, so that it contacted the vertically aligned plasmonic Au nanorods, as can be seen from the SEM image in the upper inset of Fig. 1(b). Transmittance of the composed films was studied when using a halogen lamp as a broadband p-polarized light source for a wide range of the angles of incidence, as shown schematically in the upper inset of Fig. 1(a). In the magneto-optical experiments, a DC magnetic field of 2 kOe formed by two permanent magnets was applied in the Faraday or Voigt geometries. Rotation of the magnets to 180° with respect to the sample allowed us to invert the magnetic field direction so that the magnetic contrast in the transmitted intensity or the rotation of the polarization plane was measured.

Figure 1(a) shows the wavelength-angular transmission spectrum of an array of Au nanorods prior to the deposition of nickel. It reveals two deep minima centered at approximately 540 and 820 nm that are absent in the case of bulk Au or empty AAO templates. The short wavelength minimum is associated with the *transverse* localized plasmonic resonance and corresponds to the electronic oscillations in the direction perpendicular to the long axis of nanorods [22]. As expected, the spectral position of this feature is independent of the angle of incidence. Long-wavelength transmission minimum is associated with the collective longitudinal oscillations of the electronic gas. It vanishes for normal incidence, as the projection of the fundamental field on the nanorods' axis is zero. For clarity, a cross section of this 2D spectrum for the angle of incidence of $\theta = 45°$ is shown in the lower inset of Fig. 1(a).

It turned out that the transmission spectrum of the Au/AAO nanocomposite with the nickel film on top [Fig. 1(b)] is qualitatively similar to that of the sample without nickel [Fig. 1(a)].

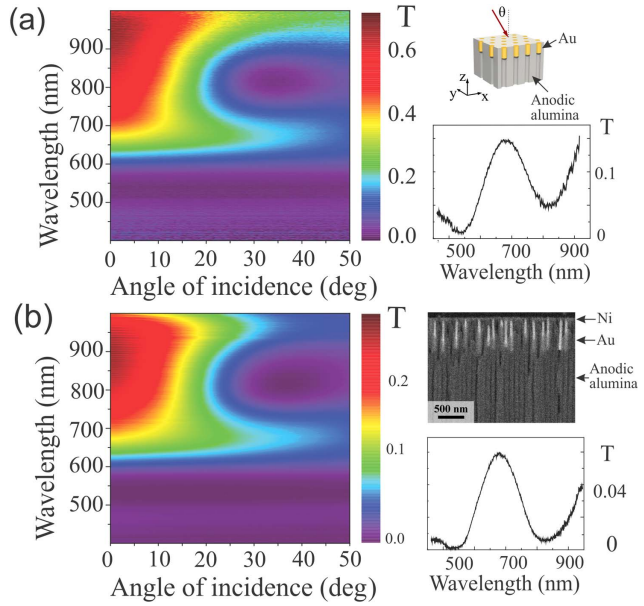

Fig. 1. Wavelength-angular transmission spectra of the array of gold nanorods (a) before and (b) after the deposition of nickel. The corresponding cross sections for the $\theta = 45°$ angle of incidence are shown in the lower insets of the figure. Upper inset to panel (a), schematic view of the experiment; upper inset to panel (b), SEM side-view image of AAO/Au nanocomposite with the thin nickel film on top.

Thus, the continuous magnetic nanolayer almost does not change the spectrum of the composite, while it decreases the overall transmission. The cross sections of the spectra of the two samples for $\theta = 45°$ are given in the lower insets of the panels (a) and (b).

Figure 2 shows the spectrum of the polarization plane rotation of the transmitted beam for the Faraday effect geometry. The scheme of the experiment is sketched in the inset of Fig. 2. Measurements were performed at normal incidence of the fundamental beam, so that only the resonance at 540 nm would appear. The spectrum reveals an enhancement of the Faraday rotation by the factor of 1.5 at the wavelength of 540 nm which correlates with the minimum of the transmission spectrum associated with the ENP spectral point. In contrast, a pure Ni film with similar parameters sputtered on an empty AAO template (red symbols in Fig. 2) does not reveal such a feature. At the same time, both structures demonstrate a monotonous increase in the Faraday effect towards the long-wavelength optical range due to the increasing absorption of nickel.

In order to reveal the magneto-optical response of the composite structure at oblique incidence, the experiments were performed in the Voigt geometry, as shown schematically in Fig. 3. In this case, the measure of the effect is the magnetic contrast defined as $\rho_\omega = \frac{T_+ - T_-}{T_+ + T_-}$, where T_+ and T_- are the transmissions for the opposite directions of the applied magnetic field, correspondingly. The spectrum of ρ_ω is presented in Fig. 3. It can be seen that nonzero ρ_ω is attained in the vicinity of the long-wavelength resonance at 840 nm only at oblique incidence, which is consistent with the theory of the transversal magneto-optical effect. It is important that close to this resonant wavelength, the magnetic contrast changes its sign, and the ρ_ω maximal absolute value reaches $5 \cdot 10^{-3}$. It should be noted that the magnetic contrast in a 15 nm thick nickel film deposited on a pure AAO template (i.e., without Au nanorods) is zero in the whole spectral range under study for this particular experimental geometry, which is consistent with the expectations [23].

The spectra of the permittivity components of the studied composite MMs were calculated within a framework of the

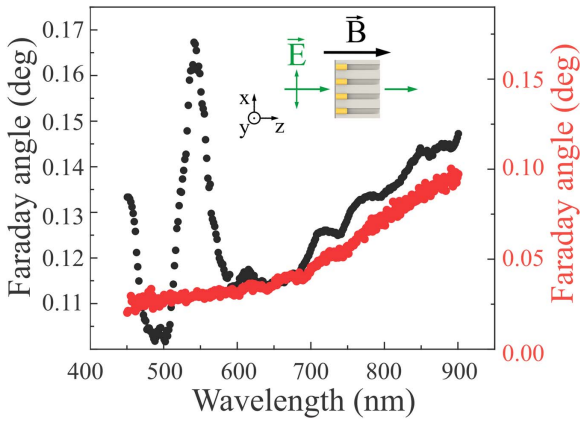

Fig. 2. Faraday rotation spectrum of the array of gold nanorods in the AAO matrix with a 15 nm thick Ni film deposited above (black points, left axis), and of the Ni film of the same thickness formed on an empty AAO template (red points, right axis). Inset: the scheme of the experiment.

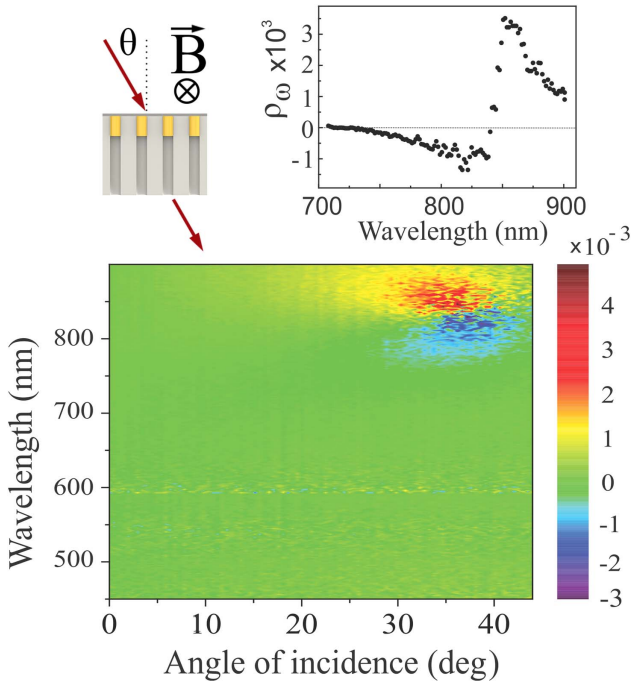

Fig. 3. Frequency-wavelength spectrum of the magnetic contrast of the array of gold nanorods situated in an anodic alumina matrix and contacting with a nickel film. The sketch of the experimental geometry and the magnetic contrast spectrum for the angle of incidence $\theta = 36°$ are shown in the upper left inset of the figure.

effective medium model accounting for the dipole-dipole interaction of the neighbor nanorods [22]. Dielectric constants of the constituent materials were taken from Ref. [24]; the volume fraction of gold (8%) and the average length of nanorods (580 nm) correspond to the parameters of the experimental samples. Figure 4(a) shows the simulated spectra of the real and imaginary parts of $\varepsilon_\perp$ and $\varepsilon_\parallel$. It can be seen that $\mathrm{Im}(\varepsilon_\perp)$ is resonantly enhanced at 540 nm wavelength, which corresponds to the absorption maximum [Fig. 4(b)] and to the experimental data (see Fig. 1). This peak is associated with the transversal plasmon excitation at $\mathrm{Re}(\varepsilon_\perp) \to \infty$.

The ENZ spectral point that corresponds to $\mathrm{Re}(\varepsilon_\parallel) \to 0$ is achieved at the wavelength of 830 nm so that, at longer wavelengths, the hyperbolic dispersion regime should be realized. The absorption spectrum [Fig. 4(b)] was calculated by means of a transfer-matrix method and reveals two spectral features centered at about 540 and 830 nm, which stays in good agreement with the experiment.

A comparison of the obtained data allows one to conclude that the two minima in transmission spectra at 540 and 830 nm are associated with ENP and ENZ points, respectively. Insufficient deviations of the spectral features from these (see Figs. 1 and 4) can be caused by imperfections of the effective medium approach used in the calculations. Besides, the permittivity of the electrodeposited Au can differ from that of the bulk material that was taken for the simulations.

Amplification of the Faraday effect observed in the vicinity of a 540 nm wavelength associated with the ENP point is caused by the resonant absorption of light due to the transversal

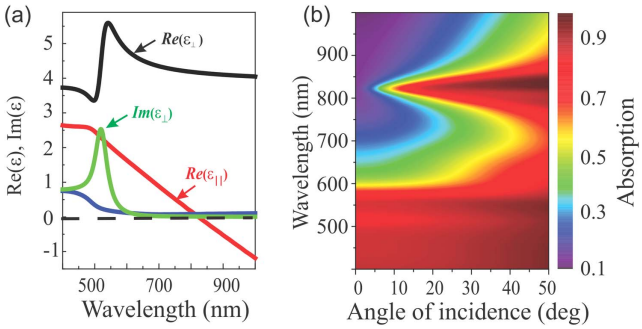

Fig. 4. Calculated spectra of the (a) permittivity tensor components $\mathrm{Re}(\varepsilon_\perp)$—black line, $\mathrm{Re}(\varepsilon_\parallel)$—red line, $\mathrm{Im}(\varepsilon_\perp)$—green line, $\mathrm{Im}(\varepsilon_\parallel)$—blue line; (b) absorption.

plasmon excitation and relevant increase of the density of states of the electromagnetic field, and corresponds to the minimum in the transmission spectrum (Fig. 1). At the same time, magnetization of the structure along the z-axis results in the appearance of nonzero off-diagonal components of the permittivity tensor $\varepsilon_{xy} = -\varepsilon_{yx}$ [23], of a y-component of the transmitted electric field and, thus, leads to the polarization plane rotation. Analogous local surface plasmon-assisted enhancement of the magneto-optical effect was observed in Au/Co/Au nanosandwiches [25] and nickel nanorods [15].

The enhancement of the magnetic contrast and the change of its sign (Fig. 4) close to the long-wavelength transmission minimum is caused evidently by magnetization induced shift of the ENZ spectral point. In reality, transversal magnetization of the Ni film leads to variation of the dielectric function of nickel and, thus, of the ENZ spectral position. The trend $\mathrm{Re}(\varepsilon_\parallel) \to 0$ leads to the enhancement of the density of states [2] and, thus, to a more effective light-matter interaction accompanied by the amplification of magnetic effects near the ENZ point.

Summing up, we studied the optical and magneto-optical effects in hyperbolic MMs composed of an ordered of Au nanorods in a porous alumina template and the same structure supplemented by a continuous Ni film that contacts the Au nanorods. Specific spectral features associated with the hyperbolic dispersion of these structures bring about two spectral resonances that are associated with the surface plasmons in Au nanorods at 540 nm and ENZ point at 830 nm, so that the hyperbolic dispersion is achieved at longer wavelengths. An enhancement of the Faraday rotation and the transversal Voigt effect was observed in the spectral vicinity of ENP and ENZ points, respectively. Further experiments on the magneto-optical effects at longer wavelengths would allow for the studies of the effect of the hyperbolic dispersion on the magneto-optical activity of MMs.

Funding. Russian Foundation for Basic Research (RFBR) (18-03-01237); President's grant (MK-5704.2018.2); M. V. Lomonosov Moscow State University Program of Development.

REFERENCES

1. M. G. Silveirinha, Phys. Rev. E **73**, 046612 (2006).
2. A. Poddubny, I. Iorsh, P. Belov, and Y. Kivshar, Nat. Photonics **7**, 948 (2013).
3. N. M. Litchinitser and V. M. Shalaev, Laser Phys. Lett. **5**, 411 (2008).
4. V. P. Drachev, W. Cai, U. Chettiar, H.-K. Yuan, A. K. Sarychev, A. V. Kildishev, G. Klimeck, and V. M. Shalaev, Laser Phys. Lett. **3**, 49 (2006).
5. P. Evans, W. R. Hendren, R. Atkinson, G. A. Wurtz, W. Dickson, A. V. Zayats, and R. J. Pollard, Nanotechnol. **17**, 5746 (2006).
6. Z. Jacob, I. Smolyaninov, and E. E. Narimanov, Appl. Phys. Lett. **100**, 181105 (2012).
7. P. Segovia, G. Marino, A. V. Krasavin, N. Olivier, G. A. Wurtz, P. A. Belov, P. Ginzburg, and A. V. Zayats, Opt. Express **23**, 30730 (2015).
8. G. Marino, P. Segovia, A. V. Krasavin, P. Ginzburg, N. Olivier, G. A. Wurtz, and A. V. Zayats, "Second-harmonic generation from hyperbolic plasmonic nanorod metamaterial slab," http://arxiv.org/abs/1508.07586 (2015).
9. Y. Sun, Zh. Zheng, J. Cheng, G. Sun, and G. Qiao, Opt. Express **23**, 6370 (2015).
10. W. Li, Zh. Liu, X. Zhang, and X. Jiang, Appl. Phys. Lett. **100**, 161108 (2012).
11. J. B. Gonzalez-Diaz, A. Garcia-Martin, G. Armelles, J. M. Garcia-Martin, C. Clavero, A. Cebollada, R. A. Lukaszew, J. R. Skuza, D. P. Kumah, and R. Clarke, Phys. Rev. B **76**, 153402 (2007).
12. I. A. Kolmychek, A. N. Shaimanov, A. V. Baryshev, and T. V. Murzina, JETP Lett. **102**, 46 (2015).
13. V. L. Krutyanskiy, I. A. Kolmychek, E. A. Gan'shina, T. V. Murzina, P. Evans, R. Pollard, A. A. Stashkevich, G. A. Wurtz, and A. V. Zayats, Phys. Rev. B **87**, 035116 (2013).
14. A. L. Chekhov, V. L. Krutyanskiy, A. N. Shaimanov, A. I. Stognij, and T. V. Murzina, Opt. Express **22**, 17762 (2014).
15. M. Pohl, L. E. Kreilkamp, V. I. Belotelov, I. A. Akimov, and A. N. Kalish, New J. Phys. **15**, 075024 (2013).
16. I. A. Kolmychek, T. V. Murzina, S. Fourier, J. Wouters, V. K. Valev, T. Verbiest, and O. A. Aktsipetrov, Solid State Phenomena **152–153**, 508 (2009).
17. T. V. Murzina, I. A. Kolmychek, A. A. Nikulin, E. A. Gan'shina, and O. A. Aktsipetrov, JETP Lett. **90**, 504 (2009).
18. D. I. Petukhov, K. S. Napolskii, and A. A. Eliseev, Nanotechnol. **23**, 335601 (2012).
19. M. Lillo and D. Losic, J. Membrane Sci. **327**, 11 (2009).
20. A. S. Vedeneev, V. V. Rylkov, K. S. Napolskii, A. P. Leontiev, A. A. Klimenko, A. M. Kozlov, V. A. Luzanov, S. N. Nikolaev, M. P. Temiryazeva, and A. S. Bugaev, JETP Lett. **106**, 411 (2017).
21. A. Mozalev, H. Baccar, and A. Abdelghani, Procedia Eng. **168**, 1188 (2016).
22. R. Atkinson, W. R. Hendren, G. A. Wurtz, W. Dickson, A. V. Zayats, P. Evans, and R. J. Pollard, Phys. Rev. B **73**, 235402 (2006).
23. A. K. Zvezdin and V. A. Kotov, *Modern Magnetooptics and Magnetooptical Materials* (Institute of Physics Publishing, 1997), p. 386.
24. E. D. Palik, *Handbook of Optical Constants of Solids* (Academic, 2012), p. 804.
25. J. B. Gonzalez-Diaz, A. Garcia-Martin, J. M. Garcia-Martin, A. Cebollada, G. Armelles, B. Sepulveda, Y. Alaverdyan, and M. Kall, Small **4**, 202 (2008).